Automotive Science and Engineering, Vol. 13, No. 1, (2023), 4041-4050

Iran University of Science and Technology

Automotive Science and Engineering

Journal Homepage: ase.iust.ac.ir

ISSN: 2008-9899

Impedance evaluation of Li-ion battery with different continuous mother wavelets: A comparative study

Mahdi Khoorishandiz, Abdollah Amirkhani*

School of Automotive Engineering, Iran University of Science and Technology

ARTICLE INFO

Article history:
Received : 5 Nov 2022
Accepted: 2 Jan 2023
Published: 28 Jan 2023

Keywords:
discrete random binary sequence
continuous wavelet transform
lithium-ion battery
dynamic time warping

A B S T R A C T

As electric vehicles become more popular, we need to keep improving the lithium-ion batteries that power them. Electrochemical impedance spectroscopy (EIS) is used based on a discrete random binary sequence (DRBS) to reduce excitation time in the low-frequency region and excite the input of the battery. In this paper, voltage and current signals are processed with wavelet transform for impedance evaluation. In using wavelet transform, choosing the most optimal mother wavelet is crucial for impedance evaluation since different mother wavelets can produce different results. We aim to compare three types of continuous Morse mother wavelet, continuous Morlet, and continuous lognormal wavelet, which are among the most important mother wavelets, to determine the best method for impedance evaluation. We used the dynamic time-warping algorithm to quantify the difference between the initial values obtained from standard laboratory equipment and the impedance evaluation through three different continuous wavelets. Our proposed method (lognormal wavelet) has the lowest difference (3.4086) from the initial values compared to the Morlet (3.5504), and Morse (3.5457) methods. As a result, our simulation shows that the lognormal wavelet transform is the best method for impedance evaluation compared to Morlet and Morse wavelets.

1. Introduction

Lithium-ion batteries are used in stationary, automotive, and portable devices due to their high energy and power density [1]. Changes in the impedance spectrum patterns of a battery analyzed through EIS, can provide information on the internal health status of major battery components (cathode, anode, and electrolyte) and the remaining useful life of the battery. In a recent paper by Zhang et al. [2], extensive testing has shown that EIS contains valuable information for detecting degradation modes and evaluating the remaining useful life of batteries. A small perturbation signal is applied to the battery input to conduct EIS, and the resulting output is measured. Mono-component sinusoidal excitation is the conventional method employed in EIS measurements [3]-[9]. Impedance calculation through EIS measurements is restricted to a finite number of frequency values. Researchers have found that the Nyquist curve provides valuable information for accurately determining a battery's real capacity, including its state of charge and state of health, in the sub-millihertz region [3], [9]. Therefore, the low-

*Corresponding Author
Email: amirkhani@iust.ac.ir
http://doi.org/10.22068/ase.2023.635

[DOI: 10.22068/ase.2023.635]

frequency region is critical for accurate battery measurement, as it can yield significant information about the battery's behavior.

When using sinusoidal excitation in EIS, it is customary to utilize 3 to 10 periods during the measurement process [10]-[12]. At low frequencies, the excitation process can become extremely time-consuming. For example, to obtain an EIS measurement at $1\,mHz$ using the recommended 3 to 10 periods, it would take between 3000 to 10000 seconds. Due to the extended stimulation period, it is difficult to prevent environmental drifts and disturbances from impacting the measurement's accuracy. In addition, achieving acceptable resolution in the extremely low-frequency domain (<10mHz) demands excessively lengthy measurement periods. For efficient EIS analysis of a wide frequency range, it is advised to employ broadband excitation signals to enable high-resolution measurements in a short period of time [13]-[19]. Research findings indicate that EIS was performed at a frequency no lower than $100\,mHz$, and the excitation process lasted approximately 90 seconds [13], [15].

This paper uses discrete random binary sequence excitation to evaluate the EIS of lithium-ion batteries. It is possible to represent a discrete random binary sequence as a sum of numerous sinusoidal signals arranged in a sequence of frequencies. Also, in this paper, wavelet transform with 3 types of mother wavelet is used to compare the evaluated values and validate EIS.

The same method was used by Li et al. [20], to estimate the Warburg-like impedance spectrum, they all used the Morlet wavelet as the mother wavelet. This method was also used by George et al. [21], to estimate the Warburg-like impedance spectrum, they all used the Morse wavelet as the mother wavelet. In this paper, we compared three types of impedance spectrum estimation methods: Morlet wavelet, Morse wavelet, and lognormal wavelet and introduced the best method for estimating the impedance spectrum. To validate the proposed EIS method, we use a recent dataset [21], this data is used on a $3.0\,Ah$ $811\,NMC-Graphite$ 18650 cylindrical lithium-ion battery of type $LG18650HG2$ $(LG\ Chem)$.

Then, using the data of the same battery [21], using DRBS stimulation, the Nyquist characteristic was evaluated by processing the voltage and current signals with Morlet wavelet, Morse wavelet, and lognormal wavelet transformations. The objective is to demonstrate that the use of time-domain signals can produce findings that match those obtained using cutting-edge laboratory equipment. Also, we evaluate the signal with the best method by comparing the three wavelets of Morlet, Morse, and lognormal.

2. Selection of the excitation signal

In order to conduct EIS on batteries using conventional methods, a set of sine waves with multi or mono components is employed to obtain EIS values at various frequencies. According to system identification principles, a noise signal with a wide frequency range, like broadband, can excite the dynamics of the system over a broad frequency band. Such a signal should have several properties: stationarity, bandwidth encompassing the highest desired frequency, and adequate power spectral density for a reliable signal-to-noise ratio [22], [23].

A signal that fulfills the properties described above can be produced using a random binary sequence. This signal alternates between two values, $+a$ and $-a$, in a random pattern. The frequency at which the value changes occur is governed by a Poisson distribution. For instance, if the intensity parameter of the Poisson distribution is set to 10, the signal will have a higher bandwidth and undergo

[DOI: 10.22068/ase.2023.635]

more frequent changes than if the intensity parameter were set to 5. Switches in discrete-time signals are constrained to occur only at discrete time points, which are determined by the minimum time between two switches λ and integer multiples of this value $k\lambda(k \epsilon \mathbb{N}^0)$ [22]. A DRBS is a collection of binary signals that are randomly distributed over time. Its time domain behavior and frequency content can be seen in FIGURE 1. The goal of using a DRBS to excite a system is to simultaneously excite the system with multiple frequencies. The optimal approach in an ideal situation is to use bandpass-limited white noise. Equation (1) illustrates the power spectral density $\Phi_x^d(\omega)$ [21].

$$\Phi_x^d(\omega) = \alpha^2\lambda \left| \frac{\sin\left(\frac{\omega\lambda}{2}\right)}{\frac{\omega\lambda}{2}} \right|^2 \qquad (1$$

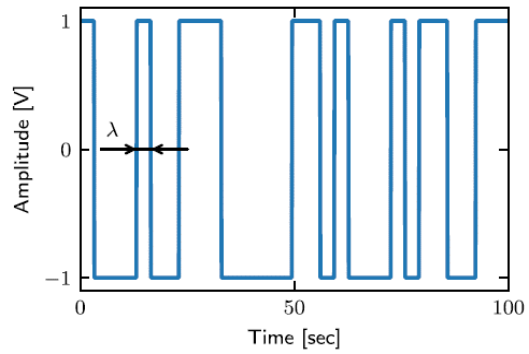

(A)

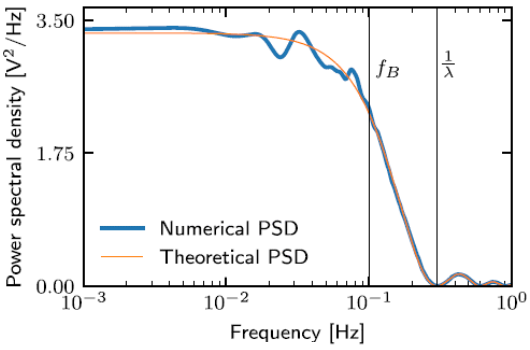

(B)

Figure 1: The DRBS generated with $\lambda = 3.3$ seconds and effective bandwidth of $f_B = 0.1Hz$ is represented by the waveform in Figure (A). The power spectral density of this sequence, obtained from a 300-second excitation, is illustrated in Figure (B).

The amplitude of the signal is represented by the letter a, while the angular frequency is denoted by ω, and the minimum time between two signal switches is called λ. The power spectrum of the signal shows a complete absence of frequencies at integer multiples of $1/\lambda$. The useful and almost flat part of the f_B frequency band is determined by the pass frequency, $-3db$, which is $f_B = 1/3\lambda$ [26]. FIGURE 1 (b) displays the power spectral density of a DRBS, which is a signal that exhibits statistical similarities to white noise [24].

3. **Wavelet transform and selecting the mother wavelet**

There are different types of mother wavelets, each of which has specific strengths and weaknesses. According to the purpose of impedance analysis, Complex mother wavelets exclusively qualify for consideration. The Morlet wavelet [27], Morse wavelet [28], [29], and lognormal wavelet [30] are the most remarkable mother wavelets utilized in the continuous wavelet transform. The time-frequency resolution is the most prevalent criterion used to select the mother wavelet [25], [26], [30]. It determines the minimum time and frequency difference needed to distinguish two mono-component sinusoidal signals in a wavelet function [25].

4. **Impedance evaluation using continuous wavelet transform**

Impedance can be determined using Continuous Wavelet Transform (CWT) just like how it is done with Fourier transform. By performing CWT on voltage $u(t)$ and current $i(t)$, one can obtain a series of complex wavelet coefficients that help in impedance analysis.

$$Wi(t,f) = \Re\{Wi(t,f)\} + j\Im\{Wi(t,f)\}$$
$$Wu(t,f) = \Re\{Wu(t,f)\} + j\Im\{Wu(t,f)\} \qquad (2$$

[DOI: 10.22068/ase.2023.635]

$Wx(t,f)$ is used to indicate the wavelet of a signal $x(t)$, and it is a function of both time t and frequency f. The impedance is determined by the ratio of the wavelet coefficients, namely $i(t)$ and $u(t)$.

$$Z(t,f) = \frac{Wu(t,f)}{Wi(t,f)} \quad (3$$

Equation 3 computes the impedance with respect to time and frequency, and it delivers the magnitude and phase at any moment and frequency point. Hence, it is viable to monitor the alterations in the phase component of impedance for every frequency over time [21].

4.1. **Initial reference measurements**

FIGURE 2 shows the initial EIS measurement curve as a black X, taken after 5 charge/discharge cycles. This curve was measured at 68 frequency points between $1mHZ$ and $10KHZ$, with 10 points per decade, each measured for 1 period. The measurement process lasted 96 minutes, with inter-frequency breaks. The impedance profile exhibits a semicircle between $3Hz$ and $5KHz$ and constant-phase capacitance properties below $3Hz$, as anticipated [21].

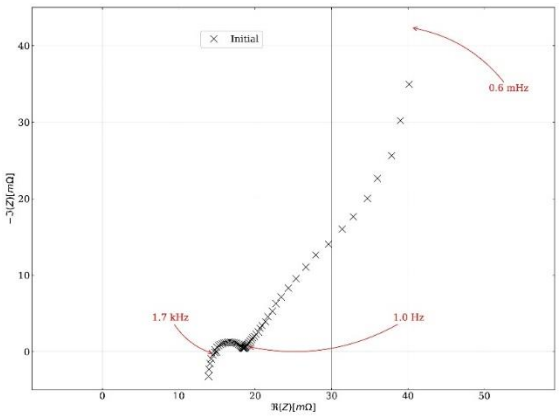

Figure 2: The initial EIS measurement curve is indicated by the black X.

4.2. **Impedance evaluation using DRBS excitation and Morlet wavelet transform**

$$\psi_{\omega 0}(t) = \pi^{-\frac{1}{4}}(e^{j\omega_0 t} - e^{-\frac{\omega_0^2}{2}})e^{-\frac{t^2}{2}} \quad (4$$

$$\Psi_{\omega 0}(t) = \pi^{\frac{1}{4}}e^{-\frac{(\omega-\omega_0)^2}{2}}(1 - e^{-\omega\omega_0}) \quad (5$$

By utilizing a recent dataset [21], impedance evaluation was conducted through discrete random binary sequence excitation to generate the Nyquist characteristic. The Morlet wavelet transform was employed to process the voltage and current signals, and the obtained data was compared with the reference values in FIGURE 3. Equations (4) and (5) were utilized to derive the Morlet wavelet and its Fourier transform.

where $\omega 0$ is the central frequency. To achieve a high level of focus in both the time and frequency domains, one can turn to the Morlet wavelet, which is a wavelet transform specifically designed for this purpose. This is accomplished by optimizing its properties to minimize the area of the Heisenberg box, which is equal to $\Delta_t \Delta_\omega = \frac{2\pi}{\sqrt{2}}$. While the Morlet wavelet is widely used in signal analysis due to its.

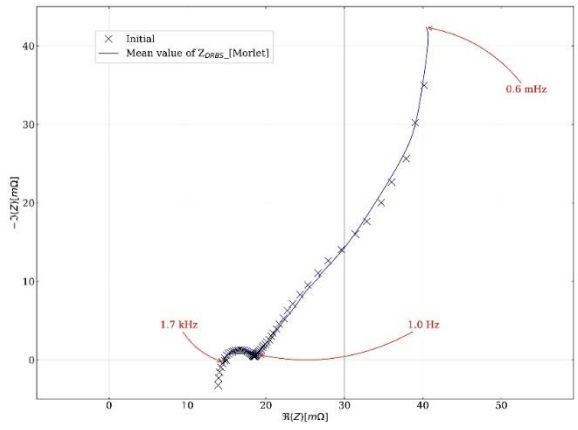

Figure 3: The comparison between the EIS measurement curve with the value evaluated using DRBS excitation and Morlet wavelet transform is shown.

strong properties, it also has some drawbacks. One of these is that it relies on a single

[DOI: 10.22068/ase.2023.635]

parameter ω_0, which can limit its flexibility. Additionally, there are restrictions on the analytical choices of this parameter when it is less than $\omega_0 < 5s^{-1}$ [28].

4.3. **Impedance evaluation using DRBS excitation and Morse wavelet transformation**

The evaluation of impedance was carried out using the most recent datasets [21], where DRBS excitation was utilized to derive the Nyquist characteristic. Morse wavelet transformation was applied to the voltage and current signals to accomplish this.

FIGURE 4 shows the comparison between data using Morse wavelet transform and reference values. The Morse wavelet in the frequency domain is defined by equation (6) [28]:

$$\Psi(\omega) = U(\omega)K_{\alpha,\beta}\omega^{\beta}e^{-\omega^{\alpha}} \quad (6$$

When computing the normalizing coefficient $K_{\alpha,\beta}$ in wavelet transforms, it is common to use the Heaviside unit step function, which is represented as $U(\omega)$. However, Morse wavelet equation (7) is used for efficient computation of the normalizing coefficient during analysis [25]:

$$\psi(\omega) = U(\omega)e^{-\omega^{\alpha}+q(\log\omega+\frac{1}{\alpha}log\frac{\alpha e}{q})} \quad (7$$

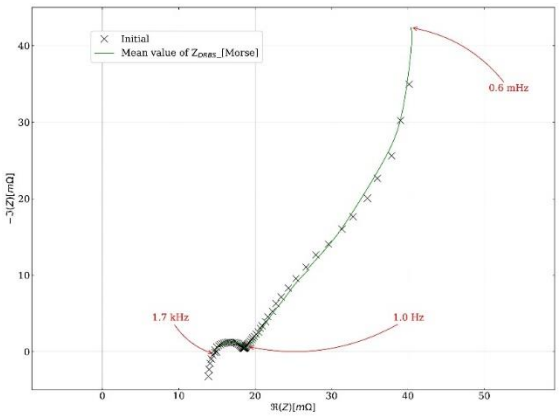

Figure 4: The comparison between the initial EIS measurement curve with the value evaluated using DRBS excitation and Morse wavelet transformation is shown.

where the parameter e represents Euler's number and q with the central frequency $\omega 0$ as $\omega 0 = \frac{q^{(1/a)}}{a}$.

4.4. **Impedance evaluation using DRBS excitation and lognormal wavelet transformation**

Impedance was evaluated using the recent dataset [21], with DRBS excitation and lognormal wavelet transformation of voltage and current signals to obtain the Nyquist characteristic. FIGURE 5 shows the comparison between the data using the lognormal wavelet transformation and the reference values. The lognormal wavelet can outperform the Morlet wavelet in certain conditions, providing better time-frequency resolution due to its logarithmic frequency resolution. The lognormal wavelet is defined by (8) [25]:

$$\hat{\psi}(\xi > 0) \sim e^{-\frac{(2\pi f_0 log\xi)^2}{2}}, \qquad \omega_{\psi} = 1 \quad (8$$

In the wavelet transformation, the resolution of f_0 parameter is akin to the Gaussian window, which is responsible for controlling the time and frequency resolution of the resulting output. The lognormal wavelet usually exhibits slightly superior resolution properties compared to the Morlet wavelet, making it "infinitely admissible." This means that all moments of the wavelet, including $\int \xi^{-n}\hat{\psi}(\xi)d\xi/\xi \ (n \geq 0)$, are finite unlike the Morlet wavelet [25].

The wavelet transform of a component enables direct reconstruction of its amplitude and phase derivatives. This feature is possible due to the analytical tractability of the wavelet, which provides explicit access to $C\psi$ and other relevant quantities [25].

Like the central frequency of the Morlet wavelet, the parameter $\omega 0$ also serves as the

[DOI: 10.22068/ase.2023.635]

central frequency in the wavelet transform . The lognormal wavelet can also achieve a computationally efficient implementation of the continuous wavelet transform through the use of frequency domain convolution using the fast Fourier transform, which is similar to the process utilized by the Morlet wavelet. The lognormal wavelet gradually improves in time-frequency resolution $\gamma_{\omega t}$, and outperforms the Morse wavelet at $er \geq 0.1$. It also has many other advantages, so it is a preferable choice among those listed in TABLE 1 [25].

Table1: Types of wavelets and their characteristics (if known analytically)

Name	Description and characteristics
Lognormal	$\hat{\psi}(\xi) = e^{-\frac{(2\pi f_0 log\xi)^2}{2}}, \quad \xi\epsilon(0,\infty)$
	$R_\psi(\omega) = \frac{1}{2}\left[\frac{\text{erf}((2\pi f_0)^{-1} log\omega)}{\sqrt{2}} + 1\right], \xi_{1,2}(\epsilon) = \exp\left[\pm\frac{n_G(\epsilon)}{2\pi f_0}\right]$
	$\omega_\psi = 1, C_\psi = \frac{\sqrt{\frac{\pi}{2}} f_0{}^{-1}}{2\pi}, D_\psi = C_\psi e^{\frac{1}{2}(4\pi^2 f_0{}^2)^{-1}}$
Morlet	$\hat{\psi}(\xi) = e^{-(\xi-2\pi f_0)^2}\left(1 - e^{-2\pi f_0 \xi}\right), \xi\epsilon(0,\infty)$
	$\psi(t) = \frac{1}{\sqrt{2\pi}} e^{-t^2/2} e^{i2\pi f_0 t} + 0\left(e^{-\frac{(2\pi f_0)^2}{2}}\right), t\epsilon(-\infty,\infty)$
	$\omega_\psi = 2\pi f_0 + 0\left(e^{-\frac{(2\pi f_0)^2}{2}}\right), D_\psi = \infty$
Generalized Morse family	$q = 30 f_0/\alpha$
	$\hat{\psi}(\xi) = B\xi^q e^{-\xi^\alpha} = e^{-\xi^\alpha + q log\xi + \log B}, \xi\ \epsilon(0,\infty), B \equiv (e\alpha/q)^{q/\alpha}$
	$D_\psi = \frac{\omega_\psi B}{2a}\Gamma((q-1)/a) (= \infty\ for\ q \leq 1)$
	$\omega_\psi = (q/a)^{1/a}, C_\psi = \frac{B}{2a}\Gamma(\text{q/a})$

The resolution parameter $f0$ for each wavelet is set so that at $f0 = 1$ they all have the same frequency resolution [25].

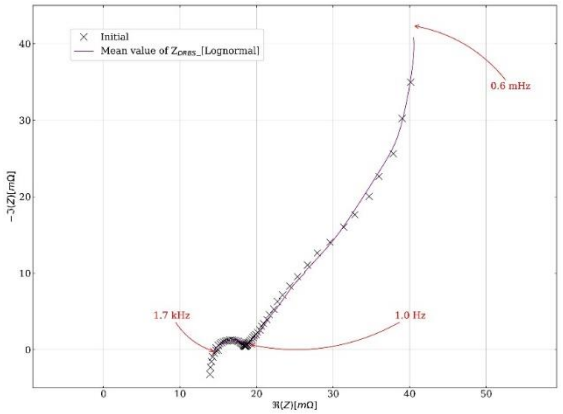

Figure 5: The comparison between the initial EIS measurement curve with the value evaluated using DRBS excitation and lognormal wavelet transformation is shown.

5. **Comparison of mother wavelets**

FIGURE 6 displays three curves on a single page to compare the performance of the three methods. To provide a more detailed analysis, we have magnified the areas with noticeable differences and presented them in FIGURES 7 and 8. As can be clearly seen in FIGURES 7 and 8, the lognormal wavelet performs better than the other two wavelet types in most points. Also, Morlet wavelets lose their analytical properties at low frequencies. To obtain accurate impedance measurements, it is essential to consider time-frequency resolution, and as such, the use of lognormal wavelets is advised.

[DOI: 10.22068/ase.2023.635]

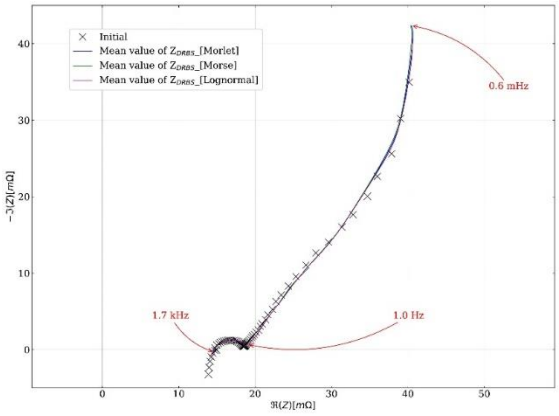

Figure 6: The comparison between the initial EIS measurement curve with the value evaluated using DRBS excitation and Morlet, Morse, and lognormal wavelet transformation is shown.

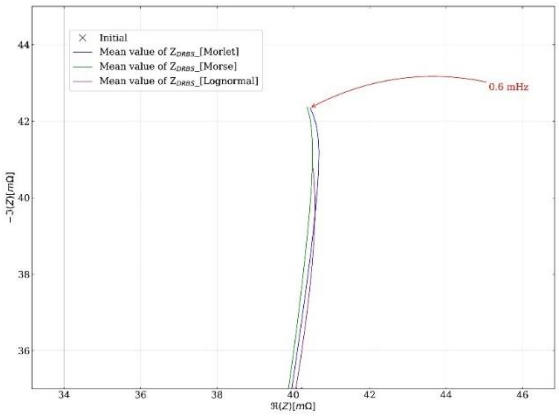

Figure 7: Magnified figure of the comparison between the initial EIS measurement curve with the value evaluated using DRBS excitation and Morlet, Morse, and lognormal wavelet transformation is shown.

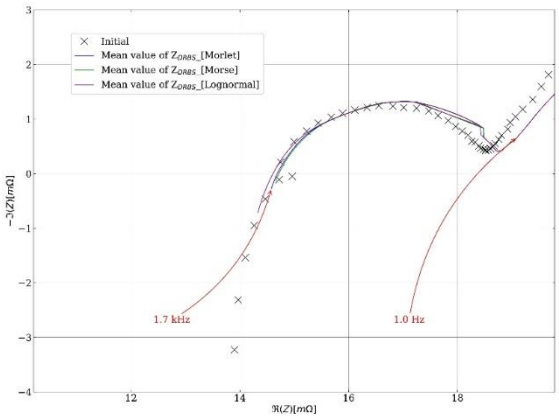

Figure 8: Magnified figure of the comparison between the initial EIS measurement curve with the value evaluated using DRBS excitation and Morlet, Morse, and lognormal wavelet transformation is shown.

6. Description of the dynamic time warping (DTW) algorithm

If two time series $Q(t)$, $P(t)$ with length M, N are assumed, we have:

$$Q(t) = q1, q2, \ldots, qM$$
$$P(t) = p1, p2, \ldots, pN \quad (9$$

To make the above signals correspond, DTW uses a matrix with dimensions of the length of two signals, whose matrix elements include the distance $Dist(i,j)$ between two points of the two signals. The distance criterion is usually defined as the distance between two signals based on DTW, $Dist(i,j) = (pi - qj)^2$, although any other criterion can also be defined.

By defining the cumulative distance $D(i,j)$, the elements of the correspondence matrix are:

$$D(i,j) = Dist(i,j) + min\begin{cases} D(i-1,j) \\ D(i-1,j-1) \\ D(i,j-1) \end{cases} \quad (10$$

the above equation shows that the twist path is calculated inversely and from the element (N,M) of the matrix. In each step, by finding the lowest value in all three paths, the correspondences are determined until finally it ends in the first layer of the matrix.

To calculate the distance between two samples of two signals, we calculate the distance based on DTW of two samples (Euclidean distance) with equation (13) as follows [31]:

$$d(x,y) = |x - y| \quad (11$$

It is also possible to calculate the distance between two signals based on DTW (squared Euclidean distance) with the following equation instead of (13) [32]:

[DOI: 10.22068/ase.2023.635]

$$d^2(x,y) = |x - y|^2 \quad (12$$

in this paper, equation (13), distance based on DTW, $d(x,y) = |x - y|$ is used**.**

7. **Comparison of mother wavelets using dynamic time Warping algorithm**

DTW (dynamic time warping) is an algorithm for measuring the similarity between two time series (signals) that may differ in speed or time. DTW is one of the powerful tools which employed in the fields of classification, data mining and regional matching of two signals. DTW can find the corresponding points based on the optimization of the distances between the points of two signals and by expanding and contracting the time axis at each point.

Table2: Comparison of mother wavelets using DTW

Mother wavelet	Distance calculated from DTW algorithm
Morlet	3.5504
Morse	3.5457
Lognormal	3.4086

Comparing the DTW distance between the reference and several different wavelets, TABLE 2 reveals that the lognormal mother wavelet has the smallest difference. This finding suggests that the lognormal wavelet is the most accurate choice for impedance evaluation.

8. **Conclusion**

The paper shows that using DRBS excitation with a lognormal wavelet for broadband EIS is a better procedure than the conventional approach using sinusoidal signals. This approach enables faster measurements and improved accuracy, as well as the ability to evaluate impedance at any frequency point using broadband excitation. Utilizing a lognormal wavelet to generate broadband excitation in system analysis enables the examination of a broad range of frequencies, providing a comprehensive understanding of the behavior of the system under study. Overall, this approach represents an important advance in the field of EIS, enabling researchers to perform more accurate and comprehensive analyses in less time. Using a tool that quickly and accurately measures impedance at low frequencies can help estimate battery health. These benefits demonstrate the usefulness of EIS based on continuous wavelet transform with a lognormal mother wavelet.

9. **Reference**

[1]X. Hu, C. Zou, C. Zhang, and Y. Li, "Technological developments in batteries: A survey of principal roles, types, and management needs," IEEE Power Energy Mag., vol. 15, no. 5, pp. 20-31, Sep. 2017.

[2]Y. Zhang, Q. Tang, Y. Zhang, J. Wang, U. Stimming, and A. A. Lee, "Identifying degradation patterns of lithium-ion batteries from impedance spectroscopy using machine learning," Nature Commun., vol. 11, no. 1, pp. 1-6, Dec. 2020.

[3] M. Oldenburger, B. Bedürftig, A. Gruhle, F. Grimsmann, E. Richter, R. Findeisen, and A.
Hintennach, "Investigation of the low-frequency Warburg impedance of Li-ion cells by frequency domain measurements," J. Energy Storage, vol. 21, pp. 272-280, Feb. 2019.

[4]M. Spielbauer, P. Berg, M. Ringat, O. Bohlen, and A. Jossen, "Experimental study of the impedance behavior of 18650 lithium-ion battery cells under deforming mechanical

[DOI: 10.22068/ase.2023.635]

abuse," J. Energy Storage, vol. 26, Dec. 2019, no. 101039.

[5] H. Dai, B. Jiang, and X. Wei, "Impedance characterization and modeling of lithium-ion batteries considering the internal temperature gradient," Energies, vol. 11, no. 1, p. 220, Jan. 2018.

[6] J. Fang, W. Shen, S. H. S. Cheng, S. Ghashghaie, H. KhurramShahzad, and C. Chung, "Fourelectrode symmetric setup for electrochemical impedance spectroscopy study of lithium-sulfur batteries," J. Power Sources, vol. 441, Nov. 2019, no. 227202.

[7] I. J. Gordon, S. Genies, G. S. Larbi, A. Boulineau, L. Daniel, and M. Alias, " Original Implementation of electrochemical impedance spectroscopy (EIS) in symmetric cells: evaluation of post-mortem protocols applied to characterize electrode materials for Li-ion batteries," J. Power sources, vol. 307, pp. 788-795, Mar. 2016.

[8] J. Li, D. Sun, X. Jin, W. Shi, and C. Sun, "Lithium-ion battery overcharging thermal characteristics analysis and an impedance-based electrothermal coupled model simulation, " Appl. Energy, vol. 254, Nov. 2019, no. 113574.

[9] X. Wang, X. Wei, H. Dai, and Q. Wu, "State estimation of lithium-ion battery based on electrochemical impedance spectroscopy with on-board impedance measurement system," in Proc. IEEE Vehicle Power Propuls. Conf. (VPPC), Oct. 2015, pp. 1-5.

[10]A. Barai, G. H. Chouchelamane, Y. Guo, A. McGordon, and P. Jennings, " A study on the impact of lithium-ion cell relaxation on electrochemical impedance spectroscopy," J. Power sources, vol. 280, pp. 74-80, Apr. 2015.

[11] F. M. Kindermann, A. Noel, S. V. Erhard, and A. Jossen, "Long-term equalization effects in Li-ion batteries due to local state of charge inhomogeneities and their impact on impedance measurements," Electrochim. Acta, vol. 185, pp. 107-116, Dec. 2015.

[12] U. Westerhoff, T. Kroker, K. Kurbach, and M. Kurrat, "Electrochemical impedance spectroscopy based estimation of the state of charge of Lithium-ion batteries," J. Energy storage, vol. 8, pp. 244-256, Nov. 2016.

[13] Y. Hoshi, N. Yakabe, K. Isobe, T. Saito, I. Shitanda, and M. Itagaki," Wavelet transformation to determine impedance spectra of lithium-ion rechargeable battery," J. Power sources, vol. 315, pp. 351-358, May 2016.

[14] A. J. Fairweather, M. P. Foster, and D. A. Stone, "VRLA battery parameter identification using pseudo-random binary sequences (PRBS)," in Proc. 5th IET Int. Conf. Power electron., Mach. Drives (PEMD), 2010, pp. 1¬-6.

[15] M. Itagaki, M. Ueno, Y. Hoshi, and I. Shitanda, "Simultaneous determination of Electrochemical impedance of lithium-ion rechargeable batteries with measurement of charge discharge curves by wavelet transformation," Electrochim. Acta, vol. 235, pp. 384389, May2017.

[16]S. M. M. Alavi, C. R. Birkl, and D. A. Howey, "Time-domaining of battery electrochemical impedance models," J. Power Sources, vol. 288, pp. 345-352, Aug. 2015.

[17]N. Lohmann, P.Weÿkamp, P. Hauÿmann, J. Melbert, and T. Musch, " Electrochemical impedance spectroscopy for lithium-ion cells: Test equipment and procedures for aging and fast characterization in time and frequency domain," J. Power Sources, vol. 273, pp. 613-623, Jan. 2015.

[18] Y. Li, J. Bao, M. Skyllas-Kazacos, M. P. Akter, X. Zhang, and J. Fletcher, "Studies on dynamic responses and impedance of the vanadium redox flow battery," Appl. Energy, vol. 237, pp. 91-102, Mar. 2019.

[DOI: 10.22068/ase.2023.635]

[19]B. Bullecks, R. Suresh, and R. Rengaswamy,"Rapid impedance measurement using chirp signals for electrochemical system analysis,"Comput. Chem. Eng., vol. 106, pp. 421 436, Nov. 2017.

[20] W. Li, Q.-A. Huang, C. Yang, J. Chen, Z. Tang, F. Zhang, A. Li, L. Zhang, and J. Zhang, " A fast measurement of Warburg-like impedance spectra with Morlet wavelet transform for electrochemical energy devices," Electrochim. Acta, vol. 322, Nov. 2019, no. 134760.

[21]Gjorgji ,Nusev, Miran Gaberšček, and Pavle Boškoski. "Fast Impedance Measurement of Li-ion Battery Using Discrete Random Binary Excitation and Wavelet Transform. " IEEE Access 9 (2021): 46152-46165.

[22]R. Isermann and M. Münchhof, Identification of Dynamic Systems: An Introduction with Applications (Advanced Textbooks in Control and Signal Processing). Berlin, germany: Springer-Verlag, 2011.

[23]L. Ljung, System Identification: Theory for the User (Prentice-Hall Information and System Sciences Series), 2nd ed. Upper Saddle River, NJ, USA: Prentice-Hall, 1999.

[24]W. D. T. Davies, System Identification for Self-Adaptive Control. New York, NY, USA: wiley, 1970.

[25]D.Iatsenko, Nonlinear Mode Decomposition. Lancashire, U.K.: Lancaster Univ., 2015.

[26]S. Mallat, A Wavelet Tour of Signal Processing: The Sparse Way, 3rd ed. Burlington, MA, USA: Academic, 2008.

[27] I. Daubechies, Ten Lectures on Wavelets, vol. 61. Philadelphia, PA, USA: SIAM, 1992.

[28]J. M. Lilly and S. C. Olhede, "Generalized morse wavelets as a superfamily of analytic wavelets," IEEE Trans. Signal Process., vol. 60, no. 11, pp. 6036-6041, Nov. 2012.

[29]S. C. Olhede and A. T. Walden, "Generalized morse wavelets," IEEE Trans. Signal Process., vol. 50, no. 11, pp. 2661-2670, Nov. 2002.

[30] D. Iatsenko, P. V. E. McClintock, and A. Stefanovska, "Linear and synchro squeezed time-frequency representations revisited: Overview, standards of use, resolution, reconstru-ction, concentration, and algorithms," Digit. Signal Process., vol. 42, pp. 1-26, Jul. 2015.

[31]Bhojwani, Mitali, and John Sahaya Rani Alex. "Field-Programmable Gate Array Implementation of the Dynamic Time Warping Algorithm for Speech Recognition." (2017).

[32]Ratanamahatana, Chotirat Ann, and Eamonn Keogh. "Everything you know about dynamic time warping is wrong." In Third workshop on mining temporal and sequential data, vol. 32. Citeseer, 2004.

[DOI: 10.22068/ase.2023.635]